© Indian Academy of Sciences

A mesoporous nickel oxide nanosheet as an electrode material for supercapacitor application using the 1-(2′,3′-dihydroxypropyl)-3-methylimidazolium hydroxide ionic liquid electrolyte

S C BHISE[1], D V AWALE[1], M M VADIYAR[1], S K PATIL[1], U V GHORPADE[1], B N KOKARE[1], J H KIM[2] and S S KOLEKAR[1],*

[1]Department of Chemistry, Analytical Chemistry and Material Science Research Laboratory, Shivaji University, Kolhapur 416004, India
[2]Department of Materials Science and Engineering and Optoelectronics Convergence Research Center, Chonnam National University, 300, Yongbong-Dong, Buk-Gu, Gwangju 500-757, South Korea
*Author for correspondence (sskolekar@gmail.com)

Abstract. NiO nanosheets were deposited on the surface of a stainless steel substrate by using a facile, environmentally friendly, reflux deposition approach for supercapacitor (SC) applications. X-ray diffraction patterns and field emission scanning electron microscopy images revealed the formation of a face centred cubic crystal structure with a uniform, compact, smoothly ordered nanosheet like structure. This study focuses on the electrochemical supercapacitive properties of NiO nanosheets with respect to cyclic voltammetry, galvanostatic charge–discharge and electrochemical impedance spectroscopy techniques in a 1-(2′,3′-dihydroxypropyl)-3-methylimidazolium hydroxide [DHPMIM][OH] ionic liquid (IL) as an electrolyte. The electrochemical study revealed that NiO (0.3 M) showed a high-specific capacitance of 205.5 F g^{-1} and an excellent cycling stability (80% specific capacitance retention after 5000 cycles) in the [DHPMIM][OH] IL electrolyte. Thus, the result showed that NiO nanosheets act as an active electrode material hold for SCs.

Keywords. Nickel oxide; supercapacitor; ionic liquid.

1. Introduction

The ever worsening energy depletion and growing concerns about air pollution and global warming have stimulated intense research on energy storage and conversion from alternative energy sources [1]. Supercapacitors (SCs), as a class of energy storage devices, are now attracting great scientific and technological interest due to their high-power density, long cycle life and low maintenance cost which make them very promising for applications in hybrid electric vehicles and other portable electronic devices [2,3]. SCs are classified into pseudocapacitors and electric double-layer capacitors (EDLCs) according to the nature of their charge storage mechanism [4]. In pseudocapacitors, fast and reversible redox reactions between the electrolyte and electro-active species on the electrode surface provide higher energy density compared with EDLCs that store charges by ion adsorption at the electrode/electrolyte interface [5,6]. RuO$_2$ has been widely studied as an active electrode material for SCs. Conversely, the expensive and toxic nature of ruthenium is inadequate for commercialization [7,8]. Therefore, much effort has been devoted to searching alternative inexpensive electrode

materials with good capacitive features, such as transition metal oxides (TMOs) and hydroxides. MnO$_2$ [9], ZnFe$_2$O$_4$ [4,10], NiO [11], Co$_3$O$_4$ [12], Ni(OH)$_2$ [13] and Co(OH)$_2$ [14,15] have been considered for pseudocapacitors due to their high-specific capacitance and also variable oxidation states for efficient redox reactions.

However, among the various TMOs, nickel oxide (NiO) has been considered as an active electrode material used in Li-ion batteries [16], fuel cells [17] and electrochemical SCs considering its Faradic pseudocapacitive performance, environmental compatibility, high-chemical and thermal stability, availability and low-cost [18,19]. There are several reports on the electrochemical performance of different NiO with different values of specific capacitance such as NiO thin films (129.5 F g^{-1} NaOH and 69.8 F g^{-1} KOH electrolyte) [20], NiO nanotubes (266 F g^{-1}) [21], NiO nanocolumns (390 F g^{-1}) [22], mesoporous NiO nanotubes (405 F g^{-1}) [23] and nanoball-like NiO (951 F g^{-1}) [24]. It has been found that the electron and ion transport efficiency for charge storage in pseudocapacitors depends on the electrode properties such as the surface morphology and surface area of NiO. NiO is a potential material used as an antiferromagnetic layer [25],

p-type transparent conducting films [26] in electrochromic devices [27] and as a functional sensor layer for chemical sensing [28]. Different methods have been used to deposit thin films of NiO such as chemical bath deposition [10], SILAR [29], spray pyrolysis [30], radio frequency magnetron sputtering [31], chemical vapour deposition [32], sol–gel [33] and electrochemical deposition methods [34].

Ionic liquids (ILs) acceptably are defined as fluid semiorganic salts composed entirely of organic cations and organic or inorganic anions at or near room temperature [35]. Recently, ILs have attracted a great deal of attention due to their high-thermal stability, good conductivity, nonflammability, suitable polarity, wide electrochemical window and recyclability [36]. Furthermore, their physical and chemical properties can be tuned by altering the cation, anion and attached substituents [37]. Recent research demonstrated that the performance of IL-based SCs is enhanced. Thus, ILs can be strategically designed for different applications. Over recent years, the concept of 'green chemistry' has become well-known among scientists worldwide. In particular, exploration of environmentally benign green solvents as alternatives to volatile organic compounds in synthesis, catalysis, extraction, separation, electrolytic processes and electrolytes in batteries, fuel cells, double layer capacitors and biosensors has been persistently pursued [35].

Therefore, the aim of this work is to understand the influence of NiO concentration on the pseudocapacitive properties. To the best of author knowledge there is no report on the electrochemical studies on NiO with the 1-(2′,3′-dihydroxypropyl)-3-methylimidazolium hydroxide [DHPMIM][OH] IL electrolyte. Herein, the study reports the deposition of NiO through a facile and environmental-friendly, reflux approach using 0.1, 0.2 and 0.3 M concentrations of nickel precursors; hereafter we call as N1, N2 and N3 with post-annealing treatment. The electrochemical data demonstrate that the specific capacitance shown by N3 is higher than that of N2 and N1, respectively, this is due to the fact that the N3 electrode possesses a higher pore volume ($0.142 \text{ cm}^3 \text{ g}^{-1}$), smaller crystallite size (47.44 nm) and good surface area ($36.3 \text{ m}^2 \text{ g}^{-1}$) in the [DHPMIM][OH] IL.

2. Experimental

2.1 *Deposition of NiO thin films*

Nickel nitrate hexahydrate ($Ni(NO_3)_2 \cdot 6H_2O$), ammonia (NH_3), 1-methylimidazole, 1-chloro-2,3-propanediol, ethyl acetate and acetone used in this work were of analytical grade (AR) and used without further purification. For the deposition of NiO thin films, the reaction bath was prepared using a $Ni(NO_3)_2 \cdot 6H_2O$ (50 ml, 0.1, 0.2 and 0.3 M concentration) precursor. To this NH_3 (28%) was added continuously with stirring, to form a clear, homogenous solution. This homogenous solution was then transferred into a round bottom flask, where the polished stainless steel (SS) substrate with zero grade polish paper was ultrasonically cleaned with double

distilled water, dipped in it and heated to reflux at 80–90°C for 2 h, after this, the solution was allowed to cool to room temperature spontaneously to deposit good quality thin films. After deposition, the films were rinsed 2–3 times in double distilled water and finally annealed at 400°C for 3 h to convert a hydroxide form into oxide form. The deposited films of NiO were uniform, well adherent and reproducible.

2.2 *Synthesis of [DHPMIM][OH] IL*

The [DHPMIM][OH] IL was synthesized in two steps. Initially, the [DHPMIM][Cl] IL was synthesized by a simple reflux method in which 0.1 mol of 1-methylimidazole and 25 ml acetone were taken in a round bottom flask and 0.15 mol of 1-chloro-2,3-propanediol was added dropwise with continuous stirring. The reaction mixture was refluxed at 65–70°C for 72 h. A yellowish viscous liquid was obtained which was purified by washing with ethyl acetate (10 ml $\times 3$) followed by *n*-hexane. Finally, the product was dried in a vacuum at 80°C for 4 h (yield 88%).

In the second step, a stoichiometric mixture of [DHPMIM] [Cl] and KOH in absolute ethanol was stirred for 45 min at room temperature. A white precipitate of KCl was separated by filtration and ethanol from the filtrate was removed by using a rotary evaporator at 80°C. A pale yellow coloured liquid of [DHPMIM][OH] IL was then dried in a vacuum at 80°C for 4 h (yield 82%) (the schematic representation of the synthesis of the [DHPMIM][OH] IL is shown in supplementary scheme 1).

2.3 *Characterization techniques*

The proton nuclear magnetic resonance (^{1}H NMR) spectrum was taken in DMSO d6 using a Bruker 300 MHz spectrophotometer. The crystal structure was determined by X-ray diffraction (XRD, Bruker D2 phaser) using an X-ray diffractometer with CuKα-radiation in the 2θ range of 20–80°C. The surface morphology was determined by field emission scanning electron microscopy (FESEM, S-4700, Hitachi). Nitrogen adsorption/desorption studies employing (Quantachrome, NOVA 1000e) instrument under a nitrogen atmosphere were carried out for determining the surface area. The oxidation states of NiO were analysed by X-ray photoelectron spectroscopy (XPS, VG Multilab 2000, Thermo VG Scientific and UK). The electrochemical properties of NiO were determined at room temperature using an electrochemical analyser (CHI608E, CH Instruments) in a three electrode cell system, where NiO was the working electrode, graphite as the counter and Ag/AgCl as reference electrodes. Cyclic voltammetry (CV) was performed in the voltage window between 0.2 and −0.9 V at different scan rates in the [DHPMIM][OH] IL electrolyte. Galvanostatic charge–discharge (GCD) was performed with different current densities. Electrochemical impedance spectroscopy (EIS) measurement was carried out by applying an AC voltage, in the frequency range from 0.01 Hz to 100 kHz in the open potential.
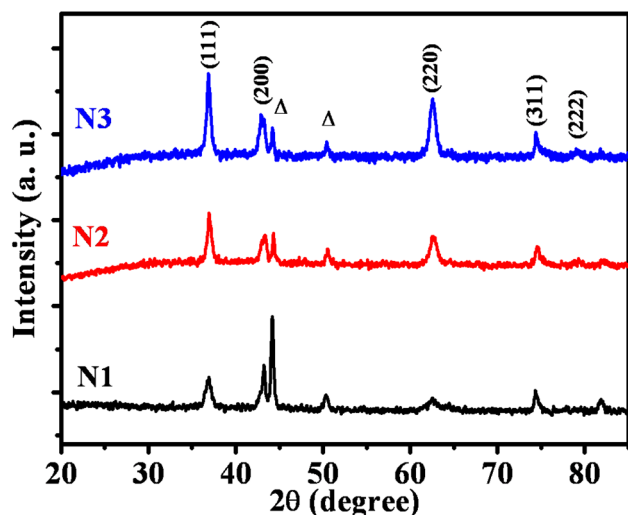
Figure 1. XRD patterns of N1, N2 and N3.

3. Results and discussion

3.1 *Characterization of IL*

The [DHPMIM][OH] IL formation was confirmed by ^{1}H NMR spectrum shown in supplementary figure S1. The obtained ^{1}H NMR data are as follows: ^{1}H NMR [DHPMIM] [OH] (DMSO, 300 MHz): δ (ppm) = 3.37–3.45 (2H, m), 3.86 (3H, s), 4.07 (1H, s), 4.09–4.14 (2H, t), 4.30 (1H, s), 4.35 (1H, s), 7.68 (2H, s), 9.15 (1H, s).

3.2 *Film formation reaction mechanism*

In the beginning, with the addition of NH_3 into the precursor solution, nickel hydroxide ($Ni(OH)_2$) precipitate formed at lower pH, which was dissolved with further addition of NH_3. Here, NH_3 acts as a complexing agent to form a nickel ammonia complex $[Ni(NH_3)_y]^{2+}$, where the free Ni^{2+} ion concentration decreases and reduces the rate of

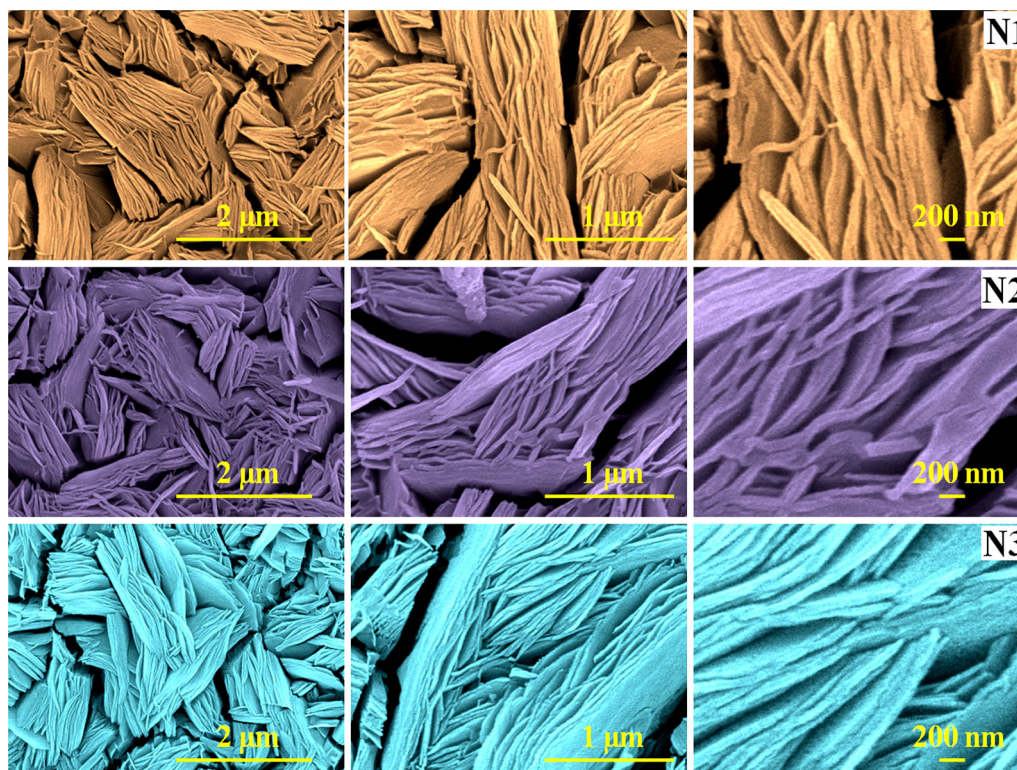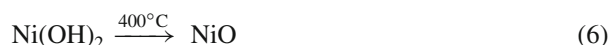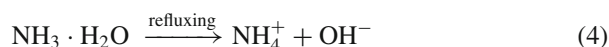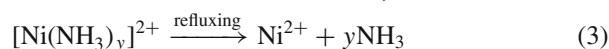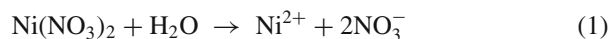**Figure 2.** FESEM images of N1, N2 and N3 at different magnifications.

Table 1. Physical and microstructural properties obtained from XRD and surface area measurements for N1, N2 and N3.

Sample	Average crystallite size (nm)	Surface area ($m^2 g^{-1}$)	Average pore diameter (nm)	Pore volume ($cm^3 g^{-1}$)
N1	47.51	21.8	7.5	0.120
N2	47.49	31.0	7.4	0.127
N3	47.44	36.3	7.1	0.142

crystal growth [38]. During reflux, a heterogeneous reaction occurs and $Ni(OH)_2$ gets deposited on the SS substrate. The α-$Ni(OH)_2$ phase is stabilized in lower-pH medium and transformed to stable β-$Ni(OH)_2$ under higher alkaline conditions [39]. $Ni(OH)_2$ is the primary skeleton of NiO. On annealing, $Ni(OH)_2$ loses water molecules to form NiO as demonstrated below [40]:

$$Ni(NO_3)_2 + H_2O \rightarrow Ni^{2+} + 2NO_3^- \qquad (1)$$

$$Ni^{2+} + yNH_3 \cdot H_2O \rightarrow [Ni(NH_3)_y]^{2+} + yH_2O \qquad (2)$$

$$[Ni(NH_3)_y]^{2+} \xrightarrow{\text{refluxing}} Ni^{2+} + yNH_3 \qquad (3)$$

$$NH_3 \cdot H_2O \xrightarrow{\text{refluxing}} NH_4^+ + OH^- \qquad (4)$$

$$Ni^{2+} + 2OH^- \xrightarrow{\text{refluxing}} Ni(OH)_2 \qquad (5)$$

$$Ni(OH)_2 \xrightarrow{400°C} NiO \qquad (6)$$

3.3 *XRD analysis*

The phase structure and crystallographic data of NiO are obtained from XRD patterns. The XRD patterns of N1, N2 and N3 are shown in figure 1. The major diffraction peaks observed at 37.22, 43.25, 62.83, 75.35 and 79.34° together with the lattice planes could be assigned to (111), (200), (220), (311) and (222). All peaks are assigned to the face centred cubic (FCC, space group (*Fm-3m*), volume cell (73.03), JCPDS card No. 01-073-1523). The diffraction peaks marked as Δ are due to the SS substrate. The crystallite size was calculated by using the Scherrer formula. The crystallite size is found to be 47.51 nm for N1, 47.49 nm for N2 and 47.44 nm for N3.

3.4 *FESEM analysis*

The surface morphology was investigated by FESEM. Figure 2 represents the FESEM images of N1, N2 and N3 at different magnifications. The FESEM images indicate the formation of a uniform, compact, smoothly ordered nanosheet like surface morphology of NiO. These results indicated that NH_3 has a pronounced impact on the surface morphology, aggregation, size and shape of NiO. As the concentration increases from N1 to N3, nucleation and growth rates are altered. This can be confirmed by surface area analysis as shown in table 1. These formed nanosheets are interconnected with each other and interlaced like petals [41]. This unique structure provides high-specific capacitance due to easy access of electrolyte ions during redox processes.

3.5 *XPS analysis*

The chemical composition and oxidation state of NiO elements were investigated by XPS. Figure 3a shows that the XPS survey spectrum of NiO mainly consists of Ni 2p, O 1s and C 1s elements. The binding energies were calibrated against the C 1s signal (284 eV) originating from the carbon
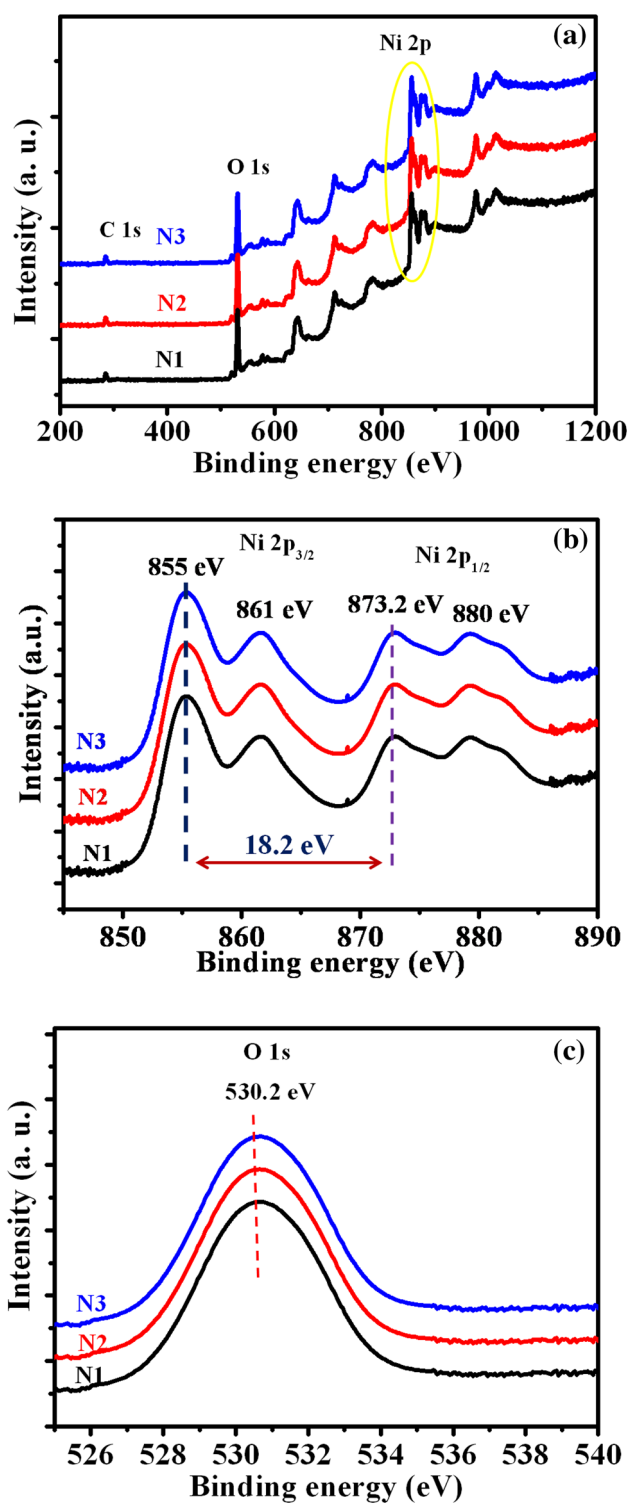
Figure 3. (**a**) Survey spectrum of N1, N2 and N3. (**b**) Core level spectrum of Ni 2p in N1, N2 and N3. (**c**) Core level spectrum of O 1s in N1, N2 and N3.

sample holder [42]. Figure 3b shows the binding energy peaks of Ni $2p_{3/2}$ and Ni $2p_{1/2}$ at 855 and 873.2 eV, with an energy separation of 18.2 eV, which are in good agreement with the reported data of Ni $2p_{3/2}$ and Ni $2p_{1/2}$ in NiO, which confirm
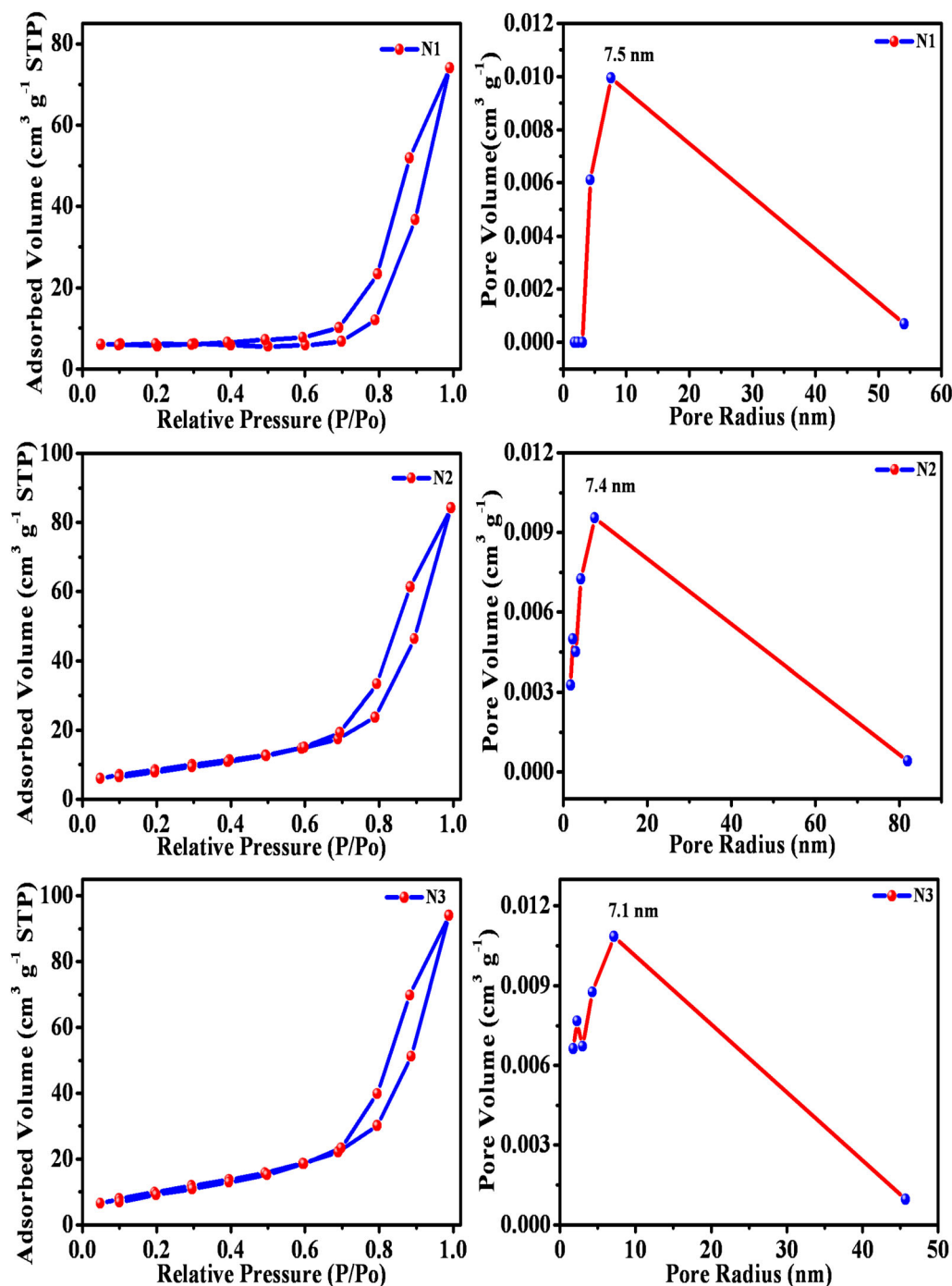
Figure 4. Nitrogen adsorption/desorption isotherms of N1, N2 and N3 and pore size distribution.

that Ni is in +2 oxidation state [43]. The core level O 1s peak at 530 eV confirms the formation of a Ni–O bond in NiO [44] as shown in figure 3c. No other peaks for other elements or impurities were observed.

3.6 *Surface area analysis*

The surface properties of N1, N2 and N3 were evaluated by Brunauer–Emmett–Teller analysis using nitrogen adsorption

isotherms and Barrett–Joyner–Halenda method for pore size distribution shown in figure 4. There is a steep uptake of nitrogen at the beginning of the measurement ($P/P_0 < 0.02$), followed by an increased uptake of gas and hysteresis. The nitrogen sorption isotherms of N1, N2 and N3 samples exhibit type IV curves (relative pressure starting from 0.4 to 0.99) and H3 hysteresis loop according to IUPAC classification, which indicates the meso or macroporous structure [45]. The specific surface area and total pore volume are tabulated in
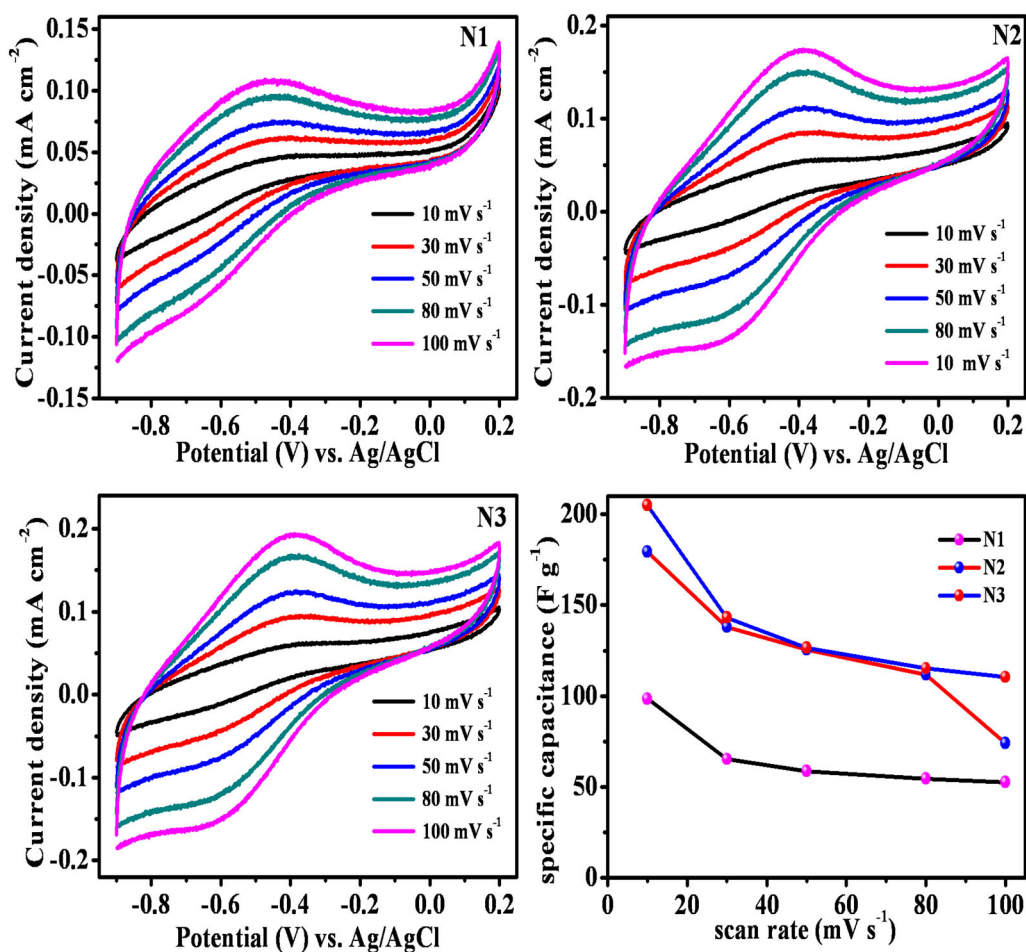
Figure 5. CV curves of N1, N2 and N3 at different scan rates and the plot of variation of specific capacitance *vs.* scan rate.

table 1. A pore size distribution as shown in figure 4 confirms that N1, N2 and N3 have mesoporous structures. The observed specific surface areas are in the order of N3 > N2 > N1.

3.7 *CV analysis*

As shown in figure 5, the CVs of the NiO nanosheets (N1, N2 and N3) at different scan rates were recorded in the potential range of 0.2 to −0.9 V in the [DHPMIM][OH] IL as an electrolyte at room temperature. The CV profiles for N1, N2 and N3 samples are very similar and quite different from the ideal rectangular shape for double-layer capacitance, which suggested that the capacitance of the NiO nanosheet primarily originates from Faradic redox reactions of NiO. The CV curves show that the anodic and cathodic peaks are due to the reversible Faradic redox reactions of Ni(I) and Ni(II) species. The oxidation and reduction peaks are shifted more towards the positive and negative axes as the scan rate increases, which is because of the fast ionic/electronic diffusion during the

Faradic redox reaction [46–48]. The redox reaction is given below as:

$$NiO + OH^- \leftrightarrow NiOOH + e^- \tag{7}$$
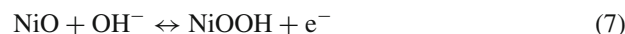
Specific capacitance was calculated from CV curves using formula [10]:

$$C = \frac{1}{m\nu(V_c - V_a)} \int_{V_a}^{V_c} I(V)\mathrm{d}V, \tag{8}$$

where m is the mass of NiO in grams, ν is the scan rate in mV s^{-1}, V_a and V_c are the anodic and cathodic potentials in volts, respectively, $I(V)$ is the response current density in ampere and V is the potential. The specific capacitance values observed for N1, N2 and N3 are 98, 65, 58, 54 and 52 F g^{-1}, 179, 137, 125, 111 and 73 F g^{-1} and 205, 143, 126, 115 and 110 F g^{-1}, respectively. The specific capacitance values of N1, N2 and N3 electrodes decreased with an increase in the scan rate as shown in figure 5. At a higher scan rate, the accessibility of OH$^-$ ions entering into the NiO, and thus the
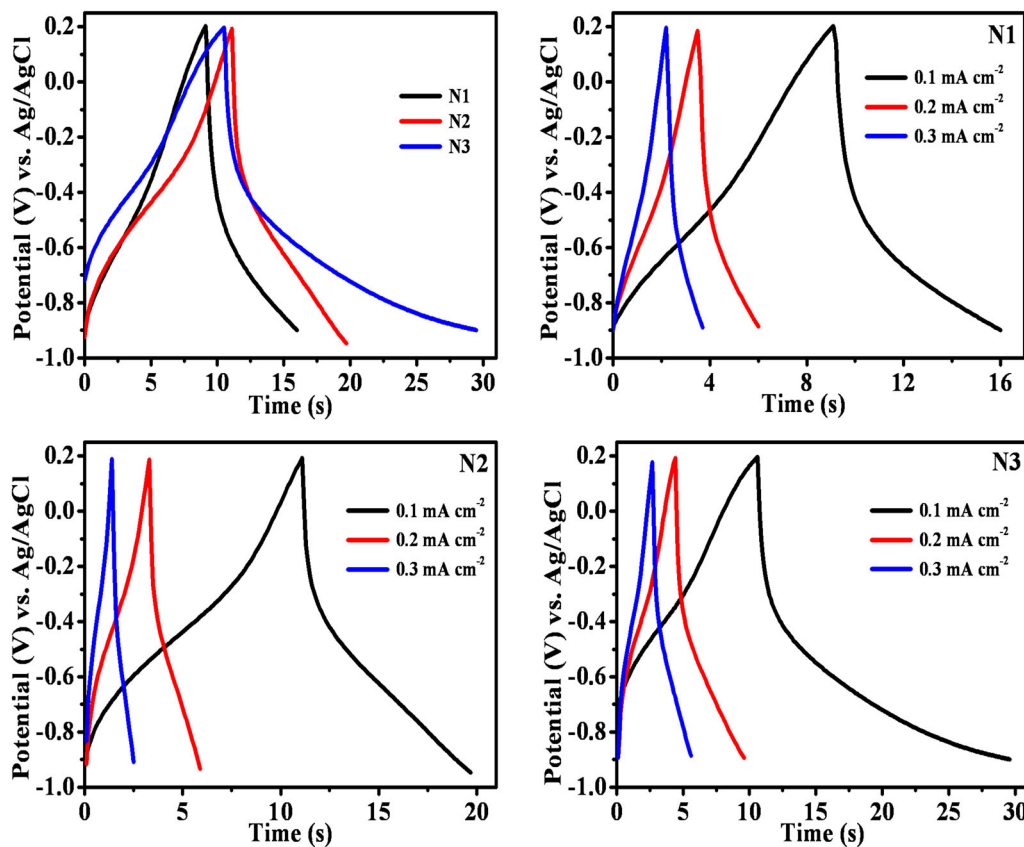
Figure 6. GCD curves of N1, N2 and N3 at a current density of 0.1 mA cm^{-2} and N1, N2 and N3 at different current densities.

transport of OH$^-$ ions was limited due to their slow diffusion. Hence, only the outer surface could be utilized for the charge storage. Thus, the N3 electrode demonstrated high-specific capacitance values by providing a more assessable surface area for redox reactions and charge storage as compared to N1 and N2 electrodes.

3.8 *GCD analysis*

To evaluate the capacitive behaviour of the NiO electrode material, the GCD measurement was investigated in the [DHPMIM][OH] IL as the electrolyte. The GCD profiles of N1, N2 and N3 electrodes were recorded at a current density of 0.1 mA cm^{-2} and different current densities as shown in figure 6. The nonlinearity in all electrodes is supporting the pseudocapacitive behaviour, as EDLCs preferably present a triangular wave like profile for a charge–discharge cycle suggesting that the NiO electrode exhibited an excellent electrochemical capacitive characteristic and remarkable reversible redox reaction. For the N3 electrode, GCD curves are substantially prolonged over the N1 and N2 electrodes and hence enhanced the capacitive performance. The better performance of the N3 electrode is due to the surface morphology (as shown in FESEM images and the
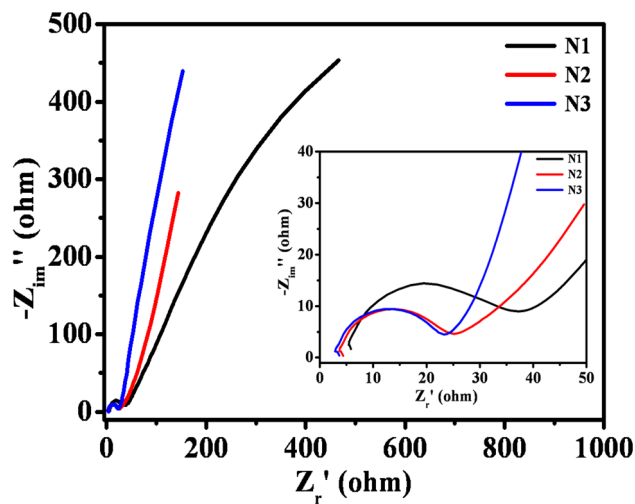
Figure 7. Nyquist plot of N1, N2 and N3 and the inset showing the magnified portion of the high-frequency region.

difference in the surface properties represented in table 1) providing more surface area and ensuring efficient diffusion path for the electrolyte ions [49].
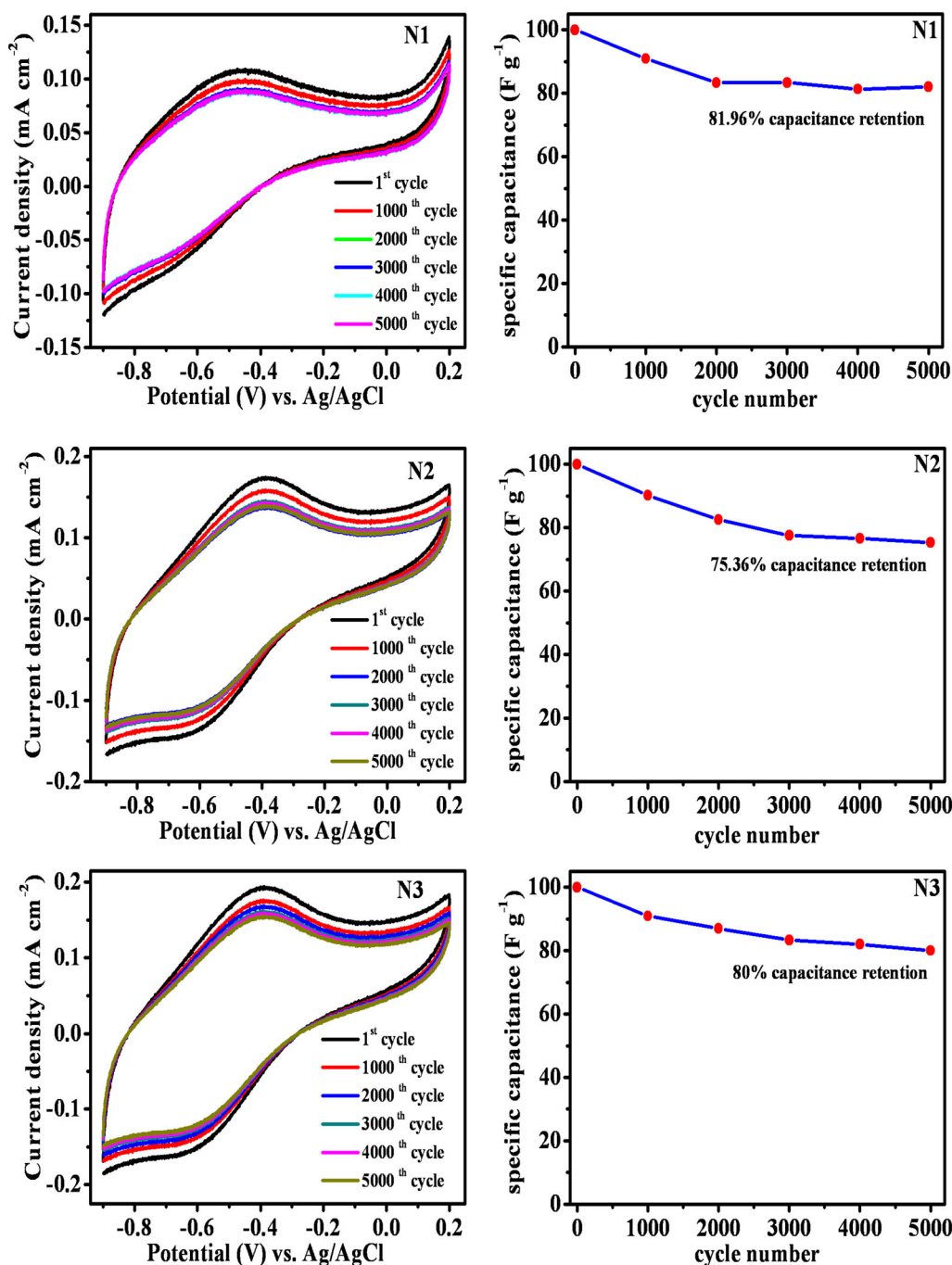
Figure 8. Stability studies of N1, N2 and N3 and plots of specific capacitance *vs.* cycle number.

3.9 *EIS analysis*

For the fundamental behaviour of the NiO nanosheet electrode for SCs, EIS measurements were carried out at the open circuit potential. Figure 7 shows the Nyquist plots of N1, N2 and N3 electrodes measured in the [DHPMIM][OH] IL as the electrolyte. The Nyquist plot is divided into a high-frequency semicircle region and straight line along the imaginary axis in the low-frequency region. The semicircle in the high-frequency region is associated with the surface

properties of the porous electrode material and corresponds to the Faradic charge transfer resistance (R_{ct}). The charge transfer resistance (combination of electrolyte accessible area and electrical conductivity) is directly related to the electro-active surface area of electrode materials. The charge transfer resistance increases in the order N3 < N2 < N1. The N3 electrode has least charge transfer resistance and shows a higher specific capacitance, due to its higher pore volume ($0.142 \ cm^3g^{-1}$), surface area ($36.3 \ m^2g^{-1}$) and smaller crystallite size ($47.44 \ nm$) (table 1). These properties of the N3

electrode make it perform a better electrode material than N2 and N1. The formation of abundant pores in the range of 1–10 nm may also enhance the diffusivity of the OH^- ions in the pore which reduces the resistance of the N3 electrode [47]. The Nyquist plot in the lower frequency range shows the diffusive resistance of the electrolyte into the interior of the electrode pores [46]. The diffusion line for the N3 electrode comes closer to an ideal straight line along the imaginary axis (Z''), indicating that the low-diffusion resistance is due to the porous network structure.

3.10 *Stability studies*

The long term cycling stability is an important requirement for the practical application in SCs. Figure 8 shows the long term cycling stability of N1, N2 and N3 nanosheets examined using a CV test at 100 mV s^{-1} from the 1st cycle up to 5000 cycles in the [DHPMIM][OH] IL electrolyte. Interestingly, the specific capacitance increases gradually at first, which can be attributed to the activation process, and then decreases slightly [18]. After 5000 cycles, the capacitance was almost retained to 81.96, 75.36 and 80% for N1, N2 and N3 as shown in figure 8 and the peak potential position changed very little, which indicates an excellent cycling stability and electrochemical reversibility. The capacitance loss is may be due to the loss of the electrical contact between the NiO and SS substrate.

4. Conclusion

In summary, a reflux approach has been adopted for the deposition of mesoporous NiO as the electrode material for the SC. Characterization of N1, N2 and N3 electrodes reflected that NiO is highly pure, uniformly deposited and has a FCC nanostructure. The electrochemical data demonstrate that the N3 electrode exhibits good pseudocapacitive behaviour due to a higher pore volume (0.142 cm^{3}g^{-1}) and smaller crystallite size (47.44 nm) with a porous nanosheet like morphology interconnected to form a network structure which enhances fast ion and electron transport and also provides a large surface area (36.3 m^{2}g^{-1}). These excellent properties make the N3 electrode suitable and more efficient for SC application.

Acknowledgements

References

[1] Wang H, Wang Y and Wang X 2012 *Electrochem. Commun.* **18** 92

[2] Wu C H, Deng S X, Wang H, Sun Y X, Liu J B and Yan H 2014 *ACS Appl. Mater. Interfaces* **6** 1106

[3] Purushothaman K, Babu I, Sethuraman B and Muralidharan G 2013 *ACS Appl. Mater. Interfaces* **5** 10767

[4] Vadiyar M M, Bhise S C, Kolekar S S, Chang J Y, Ghule K S and Ghule A V 2016 *J. Mater. Chem. A* **4** 3504

[5] Han B, Lee E, Kim J and Bang J 2015 *New J. Chem.* **39** 1996

[6] Wu Q, Liu Y and Hu Z 2013 *J. Solid State Electrochem.* **17** 1711

[7] Kim J Y, Kim K H, Kim H K, Park S H, Chung K Y and Kim K B 2014 *RSC Adv.* **4** 16115

[8] Chen P, Chen H, Qiu J and Zhou C 2010 *Nano Res.* **3** 594

[9] Yin B, Zhang S, Jiang H, Qu F and Wu X 2015 *J. Mater. Chem. A* **3** 5722

[10] Vadiyar M, Bhise S, Patil S, Patil S, Pawar D, Ghule A *et al* 2015 *RSC Adv.* **5** 45935

[11] Sun X, Wang G, Hwang J Y and Lian J 2011 *J. Mater. Chem.* **21** 16581

[12] Dam D and Lee J 2014 *ACS Appl. Mater. Interfaces* **6** 20729

[13] Tang Y, Liu Y, Yu S, Zhao Y, Mu S and Gao F 2014 *Electrochim. Acta* **123** 158

[14] Deng M, Song C, Wang C, Tseng Y, Chen J and Lu K 2015 *ACS Appl. Mater. Interfaces* **7** 9147

[15] Vadiyar M, Kolekar S, Chang J, Kashale A and Ghule A 2016 *Electrochim. Acta* **222** 1604

[16] Xiao A, Zhou S, Zuo C, Zhuan Y and Ding X 2015 *Mater. Res. Bull.* **70** 200

[17] Qiao Y, Wu X S and Li C M 2014 *J. Power Sources* **266** 226

[18] Huang M, Li F, Ji J Y, Zhang Y X, Zhao X L and Gao X 2014 *CrystEngComm* **16** 2878

[19] Singh A, Sarkar D, Khan G G and Mandal K 2014 *ACS Appl. Mater. Interfaces* **6** 4684

[20] Inamdar A I, Kim Y, Pawar S M, Kim J H, Im H and Kim H 2011 *J. Power Sources* **196** 2393

[21] Xu J, Gao L, Cao J, Wang W and Chen Z 2011 *J. Solid State Electrochem.* **15** 2005

[22] Zhang X, Shi W, Zhu J, Zhao W, Ma J, Mhaisalkar S *et al* 2010 *Nano Res.* **3** 643

[23] Xiong S, Yuan C, Zhang X and Qian Y 2011 *CrystEngComm* **13** 626

[24] Tian X, Cheng C, Qian L, Zheng B, Yuan H, Xie S *et al* 2012 *J. Mater. Chem.* **22** 8029

[25] Li B, Liu W, Zhao X G, Gong W J, Feng J N and Zhang Z D 2014 *J. Magn. Magn. Mater.* **350** 35

[26] Zhai P, Yi Q, Jian J, Wang H, Song P, Dong C *et al* 2014 *Chem. Commun.* **50** 1854

[27] Dalavi D, Devan R, Patil R, Ma Y, Kang M, Kim J *et al* 2013 *J. Mater. Chem. A* **1** 1035

[28] Yu T, Cheng X, Zhang X, Sui L, Xu Y, Gao S *et al* 2015 *J. Mater. Chem. A* **3** 11991

[29] Vadiyar M, Kolekar S, Deshpande N, Chang J, Kashale A and Ghule A 2017 *Ionics* **23** 741

[30] Ismail R, Ghafori S and Kadhim G 2013 *Appl. Nanosci.* **3** 509

[31] Chen H, Lu Y and Hwang W 2005 *Surf. Coat. Technol.* **198** 138

[32] Moravec P, Smolík J, Keskinen H, Makela J, Bakardjieva S and Levdansky V V 2011 *Mater. Sci. Appl.* **2** 258

[33] Dalavi D, Devan R, Patil R, Ma Y and Patil P 2013 *Mater. Lett.* **90** 60

[34] Azaceta E, Chavhan S, Rossi P, Paderi M, Fantini S, Ungureanu M *et al* 2012 *Electrochim. Acta* **71** 39

[35] Liu H, Liu Y and Li J 2010 *Phys. Chem. Chem. Phys.* **12** 1685

[36] Zhang S, Dokko K and Watanabe M 2015 *Chem. Sci.* **6** 3684

[37] Anouti M, Couadou E, Timperman L and Galiano H 2012 *Electrochim. Acta* **64** 110

[38] Bastakoti B P, Huang H S, Chen L C, Wu K C W and Yamauchi Y 2012 *Chem. Commun.* **48** 9150

[39] Xu L, Ding Y S, Chen C H, Zhao L, Rimkus C, Joesten R *et al* 2008 *Chem. Mater.* **20** 308

[40] Yuan C, Zhang X, Su L, Gao B and Shen L 2009 *J. Mater. Chem.* **19** 5772

[41] Pu J, Tong Y, Wang S, Sheng E and Wang Z 2014 *J. Power Sources* **250** 250

[42] Alammar T, Shekhah O, Wohlgemuth J and Mudring A V 2012 *J. Mater. Chem.* **22** 18252

[43] Liang K, Tang X and Hu W 2012 *J. Mater. Chem.* **22** 11062

[44] Yu X, Xie C, Yang L and Zhang S 2014 *Sens. Actuators B* **195** 439

[45] Cao F, Zhang F, Deng R, Hu W, Liu D, Song S *et al* 2011 *CrystEngComm* **13** 4903

[46] Singh A K, Sarkar D, Khan G G and Mandal K 2013 *J. Mater. Chem. A* **1** 12759

[47] Justin P, Meher S K and Rao G R 2010 *J. Phys. Chem. C* **114** 5203

[48] Babu G A, Ravi G, Mahalingam T, Kumaresavanji M and Hayakawa Y 2015 *Dalton Trans.* **44** 4485

[49] Gund G S, Dubal D P, Jambure S B, Shinde S S and Lokhande C D 2013 *J. Mater. Chem. A* **1** 4793